

Status of MADLOOP/aMC@NLO

Roberto Pittau *

Departamento de Física Teórica y del Cosmos
Universidad de Granada - Spain

I review the present status of the automatic NLO tools MADLOOP and aMC@NLO by presenting, as an example of their use, phenomenological studies of hadron collider processes. Perspectives on applications to linear collider Physics are also discussed.

1 Introduction

In this contribution, I review the present status of the MADLOOP [1,2] and aMC@NLO [3] projects, whose aim is computing observables at the Next to Leading Order (NLO) accuracy at high energy colliders. Both tools are based on the strategic assumption that, for the word *automation* to have its proper meaning, the only operation required from a user is that of typing-in the process to be computed, and other analysis-related information (such as final-state cuts). In particular, the codes that achieve the *automation* may only differentiate between processes depending on their general characteristics, but must never work on a case-by-case basis.

In Section 2, I review the general structure of a typical NLO calculation and the computational strategies implemented in MADLOOP. Section 3 describes the aMC@NLO framework while, in Section 4, I report on three phenomenological studies relevant at the LHC. Finally, in Section 5, I discuss the ongoing work to extend the applicability of such automatic tools to linear collider Physics.

2 MADLOOP and the problem of computing the 1-loop corrections

The typical structure of a NLO calculation is given by the following formula:

$$\sigma^{NLO} = \int_m d\sigma^B + \int_m \left(d\sigma^V + \int_1 d\sigma^A \right) + \int_{m+1} (d\sigma^R - d\sigma^A), \quad (1)$$

where $d\sigma^B$ is the Born cross section, $d\sigma^V$ is the virtual 1-loop correction, $d\sigma^R$ is the real correction, and $d\sigma^A$ and $\int_1 d\sigma^A$ are the *unintegrated* and *integrated* counterterms, respectively, which allow to compute the real contribution in 4 dimensions. The complexity of the calculation grows up rapidly with the number of external legs, especially in the sector of the 1-loop corrections. Since any 1-loop amplitude A can be decomposed in terms of known scalar 1-loop functions

$$\begin{aligned} A = & \sum_{i_0 < i_1 < i_2 < i_3}^{m-1} d(i_0 i_1 i_2 i_3) \int d^n \bar{q} \frac{1}{\bar{D}_{i_0} \bar{D}_{i_1} \bar{D}_{i_2} \bar{D}_{i_3}} + \sum_{i_0 < i_1 < i_2}^{m-1} c(i_0 i_1 i_2) \int d^n \bar{q} \frac{1}{\bar{D}_{i_0} \bar{D}_{i_1} \bar{D}_{i_2}} \\ & + \sum_{i_0 < i_1}^{m-1} b(i_0 i_1) \int d^n \bar{q} \frac{1}{\bar{D}_{i_0} \bar{D}_{i_1}} + \sum_{i_0}^{m-1} a(i_0) \int d^n \bar{q} \frac{1}{\bar{D}_{i_0}} + R, \end{aligned} \quad (2)$$

*I thank the financial support of the MICINN project FPA2011-22398 (LHC@NLO).

the problem is fully solved once one determines the set of coefficients

$$\mathcal{S} = \begin{cases} d(i_0 i_1 i_2 i_3), & c(i_0 i_1 i_2), \\ b(i_0 i_1), & a(i_0), \end{cases} \quad R. \quad (3)$$

That is obtained in MADLOOP with the OPP approach [4, 5, 6, 7, 8], in which the natural object is the *integrand* of the virtual 1-loop amplitude

$$A = \int d^d q \mathcal{A}(q). \quad (4)$$

For example, in the case of a $2 \rightarrow 4$ process, $\mathcal{A}(q)$ can be cast in the form

$$\mathcal{A}(q) = \sum \frac{N_i^{(6)}(q)}{D_{i_0} D_{i_1} \cdots D_{i_5}} + \sum \frac{N_i^{(5)}(q)}{D_{i_0} D_{i_1} \cdots D_{i_4}} + \sum \frac{N_i^{(4)}(q)}{D_{i_0} D_{i_1} \cdots D_{i_3}} + \cdots \quad (5)$$

where the $N_i^k(q)$ denote numerator functions of all possible structures with k denominators. The coefficients in Equation 3 are obtained in MADLOOP by sampling numerically the numerators $N_i^k(q)$ (considered as functions of the would-be loop momentum q) with the help of CUTTOOLS [9]. Since $N_i^k(q)$ are tree-level like objects, they are suitable to be computed with MADGRAPH, which is the tool used by MADLOOP for their numerical determination^a.

One-loop amplitudes for $2 \rightarrow n$ processes are constructed in MADLOOP by sewing *tree-level* $2 \rightarrow n + 2$ diagrams (dubbed L-cut diagrams) where one special line L is opened. Then amplitudes are formed by discarding one-loop diagrams in excess, a process that we call *diagram filtering*. Due to the 1-loop topology, two L-cut diagrams must be considered equivalent if they are identical up to a cyclic permutation, or to mirror symmetry, or to a cyclic permutation plus mirror symmetry. An example of L-cut diagram, identified with the string

$$q^* T_1 p_1^* T_2 p_2^* T_3 p_3^* T_4 q^*$$

is given in Figure 1.

The following 2 strings are equivalent to that one depicted in Figure 1

$$p_1^* T_2 p_2^* T_3 p_3^* T_4 q^* T_1 p_1^* \quad q^* T_4 p_3^* T_3 p_2^* T_2 p_1^* T_1 q^*. \quad (6)$$

It is easy to convince oneself that, when computing QCD corrections, the L-cut processes one needs to consider correspond to the following choices of the L-cut particles:

$$(q^*, \bar{q}^*) = (g, g) \quad \text{gluons,} \quad (7)$$

$$= (u, \bar{u}); (d, \bar{d}); \dots (Q, \bar{Q}) \quad \text{quarks,} \quad (8)$$

$$= (\eta, \bar{\eta}) \quad \text{ghosts.} \quad (9)$$

In general theories, the L-cuts processes corresponding to all particles in the Lagrangian should be taken into account.

^aA version working with MADGRAPH4 is available in [3], work is in progress for interfacing to MADGRAPH5 [10].

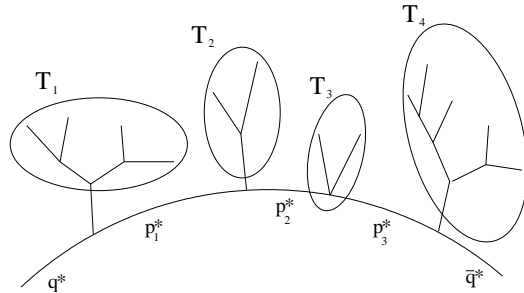


Figure 1: Example on an L-cut diagram.

3 aMC@NLO

aMC@NLO is a fully automated approach to complete event generation and subsequent parton shower at the NLO accuracy in QCD, which allows accurate and flexible simulations for both signals and backgrounds at hadron colliders. All calculational aspects in aMC@NLO are automated. One-loop contributions are evaluated with MADLOOP as described in the previous section. The other matrix-element contributions to the cross sections appearing in Equation 1, their phase-space subtractions according to the FKS formalism [11, 12], their combinations with the one-loop results, and their integration are performed by MADFKS [13]. The matching of the NLO results with HERWIG [14] or PYTHIA [15] parton showers is performed with the MC@NLO method [16], and it is also completely automatic. An important aspect of the above procedure is that all the ingredients of Equation 1 can be computed independently and put together to produce physical results in a subsequent stage ^b.

As an example of the use and validation of our automatic tools we report, in Table 1, parton level results obtained with MADFKS and MADLOOP.

4 Results at the LHC

To illustrate the kind of realistic analyses one can perform, I list here the aMC@NLO predictions for the processes $pp \rightarrow ttH$ [18], $pp \rightarrow Vbb$ [19] and $pp \rightarrow \ell^+\ell^-\ell^{(\prime)+}\ell^{(\prime)-}$ [20] at the 7 TeV LHC. Notice that an automatic procedure to determine scale and PDF uncertainties is available in the aMC@NLO framework, which allows to estimate them at almost zero CPU cost by a simple reweighting procedure. Results obtained with such a method are presented in Table 2 of Subsection 4.3.

4.1 The ttH process

The production process of a H boson in association with a top pair is a classic mechanism for Higgs production at the LHC [21, 22], where the large ttH Yukawa coupling and the presence of top quarks can be exploited to extract the signal from its QCD multi-jet background. As an example of the use of aMC@NLO for this process we present, in Figure 2, the Higgs

^bFor example, conventions exist [17] to interface real and virtual parts of a NLO computation.

	Process	μ	n_{lf}	Cross section (pb)	
				LO	NLO
a.1	$pp \rightarrow t\bar{t}$	m_{top}	5	123.76 ± 0.05	162.08 ± 0.12
a.2	$pp \rightarrow tj$	m_{top}	5	34.78 ± 0.03	41.03 ± 0.07
a.3	$pp \rightarrow tjj$	m_{top}	5	11.851 ± 0.006	13.71 ± 0.02
a.4	$pp \rightarrow t\bar{b}j$	$m_{top}/4$	4	25.62 ± 0.01	30.96 ± 0.06
a.5	$pp \rightarrow t\bar{b}jj$	$m_{top}/4$	4	8.195 ± 0.002	8.91 ± 0.01
b.1	$pp \rightarrow (W^+ \rightarrow)e^+\nu_e$	m_W	5	5072.5 ± 2.9	6146.2 ± 9.8
b.2	$pp \rightarrow (W^+ \rightarrow)e^+\nu_e j$	m_W	5	828.4 ± 0.8	1065.3 ± 1.8
b.3	$pp \rightarrow (W^+ \rightarrow)e^+\nu_e jj$	m_W	5	298.8 ± 0.4	300.3 ± 0.6
b.4	$pp \rightarrow (\gamma^*/Z \rightarrow)e^+e^-$	m_Z	5	1007.0 ± 0.1	1170.0 ± 2.4
b.5	$pp \rightarrow (\gamma^*/Z \rightarrow)e^+e^- j$	m_Z	5	156.11 ± 0.03	203.0 ± 0.2
b.6	$pp \rightarrow (\gamma^*/Z \rightarrow)e^+e^- jj$	m_Z	5	54.24 ± 0.02	56.69 ± 0.07
c.1	$pp \rightarrow (W^+ \rightarrow)e^+\nu_e b\bar{b}$	$m_W + 2m_b$	4	11.557 ± 0.005	22.95 ± 0.07
c.2	$pp \rightarrow (W^+ \rightarrow)e^+\nu_e t\bar{t}$	$m_W + 2m_{top}$	5	0.009415 ± 0.000003	0.01159 ± 0.00001
c.3	$pp \rightarrow (\gamma^*/Z \rightarrow)e^+e^- b\bar{b}$	$m_Z + 2m_b$	4	9.459 ± 0.004	15.31 ± 0.03
c.4	$pp \rightarrow (\gamma^*/Z \rightarrow)e^+e^- t\bar{t}$	$m_Z + 2m_{top}$	5	0.0035131 ± 0.0000004	0.004876 ± 0.000002
c.5	$pp \rightarrow \gamma t\bar{t}$	$2m_{top}$	5	0.2906 ± 0.0001	0.4169 ± 0.0003
d.1	$pp \rightarrow W^+W^-$	$2m_W$	4	29.976 ± 0.004	43.92 ± 0.03
d.2	$pp \rightarrow W^+W^- j$	$2m_W$	4	11.613 ± 0.002	15.174 ± 0.008
d.3	$pp \rightarrow W^+W^+ jj$	$2m_W$	4	0.07048 ± 0.00004	0.1377 ± 0.0005
e.1	$pp \rightarrow HW^+$	$m_W + m_H$	5	0.3428 ± 0.0003	0.4455 ± 0.0003
e.2	$pp \rightarrow HW^+ j$	$m_W + m_H$	5	0.1223 ± 0.0001	0.1501 ± 0.0002
e.3	$pp \rightarrow HZ$	$m_Z + m_H$	5	0.2781 ± 0.0001	0.3659 ± 0.0002
e.4	$pp \rightarrow HZ j$	$m_Z + m_H$	5	0.0988 ± 0.0001	0.1237 ± 0.0001
e.5	$pp \rightarrow Ht\bar{t}$	$m_{top} + m_H$	5	0.08896 ± 0.00001	0.09869 ± 0.00003
e.6	$pp \rightarrow Hb\bar{b}$	$m_b + m_H$	4	0.16510 ± 0.00009	0.2099 ± 0.0006
e.7	$pp \rightarrow Hjj$	m_H	5	1.104 ± 0.002	1.036 ± 0.002

Table 1: Results for total rates, possibly within cuts, at the 7 TeV LHC, obtained with MADFKS and MADLOOP. The errors are due to the statistical uncertainty of Monte Carlo integration.

transverse momentum distribution and the transverse momentum of the ttH or ttA system for a standard model (scalar) Higgs with $M_H = 120$ GeV and for a pseudoscalar one with $M_A = 120/40$ GeV. The total NLO cross sections in the three cases are $\sigma_{\text{NLO}}(M_H = 120) = 103.4$ fb, $\sigma_{\text{NLO}}(M_A = 120) = 31.9$ fb, and $\sigma_{\text{NLO}}(M_A = 40) = 77.3$ fb, respectively. At moderate values of the Higgs transverse momentum, the scalar and pseudoscalar cases are clearly distinguishable, while at larger values the three distributions tend to coincide. Parton shower effects give in general small corrections with respect to the a pure NLO calculation, except for variables involving all produced particles, such as the transverse momentum of the ttH or ttA system shown in the right panel of Figure 2.

4.2 The Vbb process

With Vbb we understand $\ell\nu b\bar{b}$ and $\ell^+\ell^- b\bar{b}$ final states, which are the main backgrounds to searches for SM Higgs production in association with vector bosons (WH/ZH), with the subsequent Higgs decay into a $b\bar{b}$ pair. The aMC@NLO framework allows a realistic study

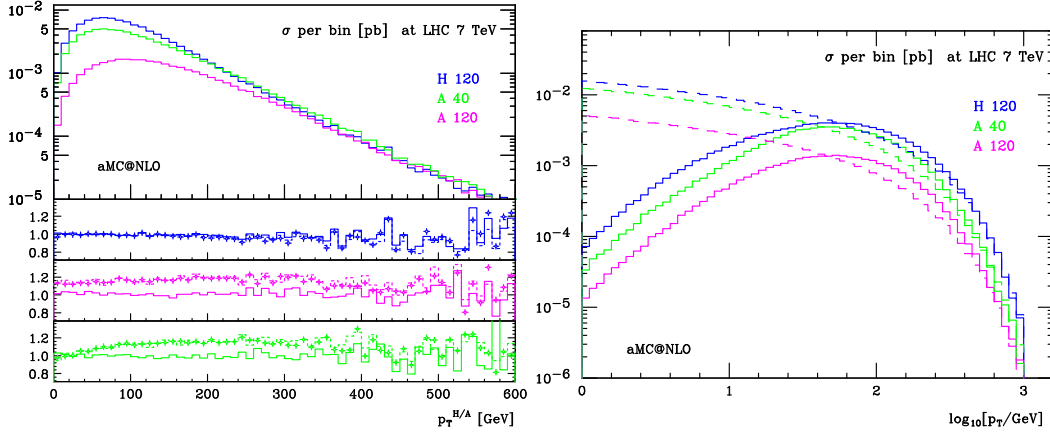


Figure 2: Higgs transverse momentum distributions (left) and transverse momentum of the ttH or ttA system (right) in ttH/ttA events at the LHC ($\sqrt{s}=7$ TeV), with aMC@NLO in the three cases: Scalar (blue) and pseudoscalar (magenta) Higgs with $m_{H/A} = 120$ GeV and pseudoscalar (green) with $m_A = 40$ GeV. In the lower panels of the left part, the ratios of aMC@NLO over LO (dashed), NLO (solid), and aMC@LO (crosses) are shown. Solid histograms in the right panel are relevant to aMC@NLO, dashed ones to a pure NLO calculation.

including

- NLO corrections;
- bottom quark mass effects;
- spin-correlation and off-shell effects;
- showering and hadronization.

As an example we show, in Figure 3, the invariant mass of the pair of the two leading b-jets, compared with the signal distributions for a standard Higgs with $m_H = 120$ GeV. Figure 3 is interesting because both signal and background are studied at the NLO accuracy.

4.3 Four-lepton production

Vector boson pair production is important in at least two respects. Firstly, it is an irreducible background to Higgs signals, in particular through the W^+W^- and ZZ channels which are relevant to searches for a standard model Higgs of mass larger than about 140 GeV. Secondly, di-boson cross sections are quite sensitive to violations of the gauge structure of the standard model, and hence are good probes of scenarios where new Physics is heavy and not directly accessible at the LHC, yet the couplings in the vector boson sector are affected. The neutral process

$$pp \rightarrow (Z/\gamma^*)(Z/\gamma^*) \rightarrow \ell^+ \ell^- \ell^{(\prime)+} \ell^{(\prime)-}$$

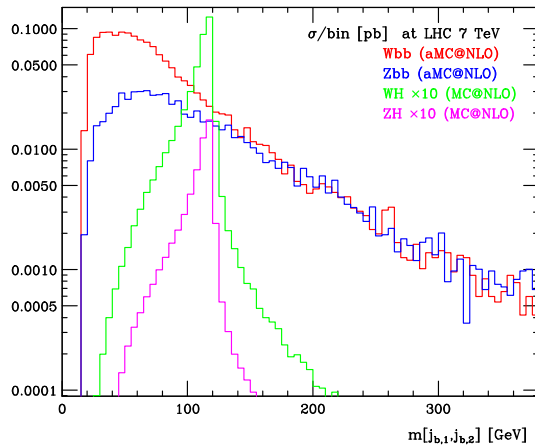


Figure 3: Invariant mass of the pair of the two leading b -jets. $WH(\rightarrow \ell\nu bb)$, $ZH(\rightarrow \ell^+\ell^-bb)$, $\ell\nu bb$, and $\ell^+\ell^-bb$ results are shown, with the former two rescaled by a factor of ten.

is considered here, which, although smaller than the W^+W^- channel, may provide a cleaner signal due to the possibility of fully reconstructing the decay products of the two vector bosons. aMC@NLO predictions for the cross sections are given in Tab. 2, which, as already mentioned, also includes aMC@NLO estimates for scale and PDF uncertainties. The four-lepton invariant mass and the transverse momentum distribution are presented in Figure 4, where comparisons between the results obtained with aMC@NLO matched to HERWIG and to PYTHIA are also given. I stress that these results include the contributions due to gg -initiated processes, which have also been computed automatically. These are formally of NNLO, but may play a non-negligible phenomenological role owing to their parton-luminosity dominance at a large-energy collider such as the LHC.

Process	Cross section (fb)		
	$q\bar{q}/qg$ channels		gg channel
	$\mathcal{O}(\alpha_s^0)$	$\mathcal{O}(\alpha_s^0) + \mathcal{O}(\alpha_s)$	$\mathcal{O}(\alpha_s^2)$
$pp \rightarrow e^+e^-\mu^+\mu^-$	9.19	$12.90^{+0.27(2.1\%)+0.26(2.0\%)}_{-0.23(1.8\%)-0.22(1.7\%)}$	$0.566^{+0.162(28.6\%)+0.012(2.1\%)}_{-0.118(20.8\%)-0.014(2.5\%)}$
$pp \rightarrow e^+e^-e^+e^-$	4.58	$6.43^{+0.13(2.1\%)+0.11(1.7\%)}_{-0.13(2.0\%)-0.10(1.6\%)}$	

Table 2: Total cross sections for $e^+e^-\mu^+\mu^-$ and $e^+e^-e^+e^-$ production at the LHC ($\sqrt{S} = 7$ TeV) within the cuts $M(\ell^\pm\ell'^{\mp}) \geq 30$ GeV. The first and second errors affecting the results are the scale and PDF uncertainties (also given as fractions of the central values).

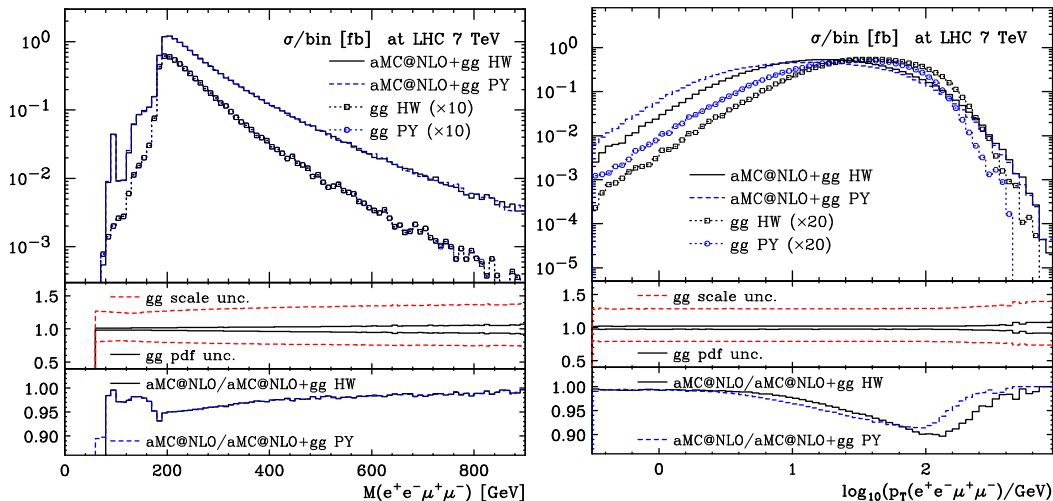


Figure 4: Four-lepton invariant mass and the transverse momentum distributions for aMC@NLO+ gg HERWIG (solid black) and PYTHIA (dashed blue) results. The rescaled gg contributions with HERWIG (open black boxes) and PYTHIA (open blue circles) are shown separately. Middle insets: scale (dashed red) and PDF (solid black) fractional uncertainties. Lower insets: aMC@NLO/(aMC@NLO+ gg) with HERWIG (solid black) and PYTHIA (dashed blue).

5 Perspectives for linear collider Physics

Automatic tools such as those described in the previous sections can be successfully employed for studying ILC/CLIC e^+e^- Physics as well. However, for this to be achieved in practice, a number of intermediate technical challenges should be dealt with. If, on the one hand, the treatment of the real radiation is much easier due to the much simpler initial state, on the other hand, the need of including the full set of electroweak 1-loop corrections could pose a problem in terms of speed due to the much larger number of contributing Feynman diagrams. If, in addition, one wishes to study SUSY or generic BSM models at linear colliders including radiative corrections, things can become too slow. However, one should not forget that the intrinsic simplicity of the algorithms used in MADLOOP and aMC@NLO is, at a very large extent, independent on the complexity of the process under study and that the results are always guaranteed to be correct thanks to the complete automation of the whole procedure. Therefore, simple caching strategies and a clever organization of the calculation can be used to deal with such CPU challenging computations. Finally, the fact that both MADLOOP and aMC@NLO are embedded into the MADGRAPH framework guarantees a dedicated and constant work in the direction of extending them to theories more complicated than QCD. For example, the complete electroweak standard model in the renormalizable gauge is being currently implemented in MADGRAPH5, together with the ultraviolet counterterms and the needed so called R_2 finite renormalization [23, 24]. Work is also in progress for SUSY and BSM theories [25, 26, 27].

6 Conclusion

Physics at the Next-to-Leading order accuracy should be easy and the tools dedicated to its study at high-energy colliders user friendly. In order to allow a quick progress in our understanding of the fundamental laws of nature, the human effort should be better employed to compare easily produced theoretical predictions with data.

References

- [1] V. Hirschi, R. Frederix, S. Frixione, M. V. Garzelli, F. Maltoni and R. Pittau, JHEP **1105** (2011) 044 [arXiv:1103.0621 [hep-ph]].
- [2] V. Hirschi, arXiv:1111.2708 [hep-ph].
- [3] <http://amcatnlo.cern.ch>.
- [4] G. Ossola, C. G. Papadopoulos and R. Pittau, Nucl. Phys. B **763** (2007) 147 [hep-ph/0609007].
- [5] G. Ossola, C. G. Papadopoulos and R. Pittau, JHEP **0707** (2007) 085 [arXiv:0704.1271 [hep-ph]].
- [6] G. Ossola, C. G. Papadopoulos and R. Pittau, JHEP **0805**, 004 (2008) [arXiv:0802.1876 [hep-ph]].
- [7] P. Draggiotis, M. V. Garzelli, C. G. Papadopoulos and R. Pittau, JHEP **0904** (2009) 072 [arXiv:0903.0356 [hep-ph]].
- [8] R. Pittau, Comput. Phys. Commun. **181** (2010) 1941 [arXiv:1006.3773 [hep-ph]].
- [9] G. Ossola, C. G. Papadopoulos and R. Pittau, JHEP **0803** (2008) 042 [arXiv:0711.3596 [hep-ph]].
- [10] J. Alwall, M. Herquet, F. Maltoni, O. Mattelaer and T. Stelzer, JHEP **1106** (2011) 128 [arXiv:1106.0522 [hep-ph]].
- [11] S. Frixione, Z. Kunszt and A. Signer, Nucl. Phys. B **467** (1996) 399 [hep-ph/9512328].
- [12] S. Frixione, JHEP **1109** (2011) 091 [arXiv:1106.0155 [hep-ph]].
- [13] R. Frederix, S. Frixione, F. Maltoni and T. Stelzer, JHEP **0910** (2009) 003 [arXiv:0908.4272 [hep-ph]].
- [14] G. Corcella, I. G. Knowles, G. Marchesini, S. Moretti, K. Odagiri, P. Richardson, M. H. Seymour and B. R. Webber, JHEP **0101** (2001) 010 [hep-ph/0011363].
- [15] T. Sjostrand, S. Mrenna and P. Z. Skands, JHEP **0605** (2006) 026 [hep-ph/0603175].
- [16] S. Frixione and B. R. Webber, JHEP **0206** (2002) 029 [hep-ph/0204244].
- [17] T. Binoth, F. Boudjema, G. Dissertori, A. Lazopoulos, A. Denner, S. Dittmaier, R. Frederix and N. Greiner *et al.*, Comput. Phys. Commun. **181** (2010) 1612 [arXiv:1001.1307 [hep-ph]].
- [18] R. Frederix, S. Frixione, V. Hirschi, F. Maltoni, R. Pittau and P. Torrielli, Phys. Lett. B **701** (2011) 427 [arXiv:1104.5613 [hep-ph]].
- [19] R. Frederix, S. Frixione, V. Hirschi, F. Maltoni, R. Pittau and P. Torrielli, JHEP **1109** (2011) 061 [arXiv:1106.6019 [hep-ph]].
- [20] R. Frederix, S. Frixione, V. Hirschi, F. Maltoni, R. Pittau and P. Torrielli, arXiv:1110.4738 [hep-ph].
- [21] S. Dittmaier *et al.* [LHC Higgs Cross Section Working Group Collaboration], arXiv:1101.0593 [hep-ph].
- [22] S. Dittmaier, S. Dittmaier, C. Mariotti, G. Passarino, R. Tanaka, S. Alekhin, J. Alwall and E. A. Bagnaschi *et al.*, arXiv:1201.3084 [hep-ph].
- [23] M. V. Garzelli, I. Malamos and R. Pittau, JHEP **1001** (2010) 040 [Erratum-ibid. **1010** (2010) 097] [arXiv:0910.3130 [hep-ph]].
- [24] M. V. Garzelli, I. Malamos and R. Pittau, JHEP **1101** (2011) 029 [arXiv:1009.4302 [hep-ph]].
- [25] N. D. Christensen and C. Duhr, Comput. Phys. Commun. **180** (2009) 1614 [arXiv:0806.4194 [hep-ph]].
- [26] C. Degrande, C. Duhr, B. Fuks, D. Grellscheid, O. Mattelaer and T. Reiter, arXiv:1108.2040 [hep-ph].
- [27] R. Pittau, JHEP **1202** (2012) 029 [arXiv:1111.4965 [hep-ph]].